Applied Catalysis B: Environmental 239 (2018) 450–462

Contents lists available at ScienceDirect

Applied Catalysis B: Environmental

journal homepage: www.elsevier.com/locate/apcatb

Sol-gel entrapped Au^0- and Ag^0-nanoparticles catalyze reductive de-halogenation of halo-organic compounds by BH_4^-

Jaydeep Adhikary[a,*], Dan Meyerstein[a,b,*], Vered Marks[a], Michael Meistelman[c], Gregory Gershinsky[d], Ariela Burg[e], Dror Shamir[f], Haya Kornweitz[a], Yael Albo[c,**]

[a] Chemical Sciences Dept., Ariel University, Ariel, Israel
[b] Chemistry Dept., Ben-Gurion University, Beer-Sheva, Israel
[c] Chemical Engineering, Biotechnology and Materials Dept., Ariel University, Ariel, Israel
[d] Institute for Nanotechnology and Advanced Materials, Bar-Ilan University, Israel
[e] Chemical Engineering Dept., Sami Shamoon College of Engineering, Beer-Sheva, Israel
[f] Chemistry Dept., Nuclear Research Centre Negev, Beer-Sheva, Israel

ARTICLE INFO

Keywords:
Sol-gel
Silica matrix
Gold and silver nanoparticles
Dehalogenation
Mechanistic study

ABSTRACT

This study investigated the reductive de-halogenations of toxic $Br_3CCO_2^-$, $Br_2CHCO_2^-$, $BrCH_2CO_2^-$, $CH_3CHBrCO_2^-$, $CH_2BrCH_2CO_2^-$, $CH_2BrCHBrCO_2^-$, $Cl_3CCO_2^-$, Cl_2CHCO_2- and $ClCH_2CO_2^-$ by sodium borohydride catalyzed by sol-gel silica entrapped Au^0 and Ag^0 nanoparticles. The results indicate that the mechanism of reduction of $Br_3CCO_2^-$ differs from that of $Cl_3CCO_2^-$. Calculated by DFT, the source of this difference lies in the larger bond strength of C—Cl compared to that of C—Br and the weaker M^0—C bond strength in Au^0-$CBr_2CO_2^-$ compared to those of Au^0-$CCl_2CO_2^-$ and Au^0-$CH_2CO_2^-$. Furthermore, the de-halogenation mechanisms catalyzed by Ag^0-NPs differ from those catalyzed by Au^0-NPs. The latter observation is attributed to the different Ag—C and Au—C bond strengths and to the different over-potentials for H_2 release of these M^0-NPs. In addition, product composition depends on the rate of BH_4^- addition. Proton labeling experiments prove that nearly all the hydrogen atoms in the products originated from the water solvent and not from the BH_4^-. The detailed mechanistic conclusions that can be drawn from these results differ considerably from those commonly accepted for de-halogenation processes.

1. Introduction

Halogenated organic compounds are widely used as starting materials, intermediates and solvents in the chemical industry, in agricultural chemistry, and in medicinal chemistry [1,2]. Considered major environmental pollutants [3], however, representatives of these chemicals comprise most of the top one hundred species in the list of hazardous compounds [4,5]. Chief among the halo-organic compounds are halo-acetic acids (HAAs), whose toxicity, strong bioaccumulation and persistence constitute significant threats to the environment and to human health through, among other things, their deleterious effects on water quality [6]. The formation of these halo-acetic acids (HAAs) during the treatment of water and wastewater with chlorine or bromine for disinfection purposes is the most significant source of halo-acetic acids in wastewater [7,8]. The U.S. Environmental Protection Agency proposed a maximum contaminant level of 60 μg/L for the sum of the concentrations of five HAAs, i.e., mono-chloro-acetic acid (MCAA), di-chloro-acetic acid (DCAA), tri-chloro acetic acid (TCAA), mono-bromo-acetic acid (MBAA) and di-bromo-acetic acid (DBAA) [9]. Typical halogenated disinfection by-products, exhibit high toxicity, geno-toxicity, and carcinogenicity [10]. Consequently, researchers the world over are working to develop a viable method for their removal from waste streams [11]. Recently it was shown that gold metal nanoparticles (Au^0-NPs) entrapped in SiO_2 sol-gel matrices catalyze the de-halogenation of HAAs by BH_4^- [12]. The results indicated that the mechanisms of these degradation processes depend on the rate of BH_4- addition and differ for the de-halogenation of Cl_3CCO_2- and $Br_3CCO_2^-$ [12a]. It is commonly assumed that the de-halogenation of X_3CCO_2- proceeds in steps, wherein X_2CHCO_2- and XCH_2CO_2- are formed as successive intermediates [13]. However, recent results for the Au^0-NPs catalyzed de-bromination of $Br_3CCO_2^-$ suggested that this is not always the case [12a], where de-bromination of Br_3CCO_2- is leading to succinic acid

* Corresponding authors at: Chemical Sciences Dept., Ariel University, Ariel, Israel.
** Corresponding author.
E-mail addresses: adhikaryj86@gmail.com (J. Adhikary), danmeyer@bgu.ac.il (D. Meyerstein), yaelyt@ariel.ac.il (Y. Albo).

https://doi.org/10.1016/j.apcatb.2018.08.040
Received 17 April 2018; Received in revised form 1 August 2018; Accepted 17 August 2018
Available online 18 August 2018
0926-3373/

and acetic acid whereas the only product of the de-chlorination of Cl_3CCO_2- is acetic acid. The detailed sources of these differences were not elucidated, though they are expected to lead to the development of more efficient catalytic de-halogenation processes.

Fe^0-NPs (ZVI) are commonly used to de-halogenate a variety of halo-organic compounds, both in batch processes and by injecting ZVI into underground polluted water streams [14]. However, these processes are slow and, moreover, result in the release of iron ions into the waste streams. A potential solution to these problems comprises the use of noble metal nanoparticles (M^0-NPs) for the de-halogenation of HAAs, as M^0-NPs have already been applied successfully in diverse applications across a range of fields, e.g., in catalysis [15], sensors [16], optics [17] and fuel cells [18]. Gold and silver nanoparticles were shown to catalyze the de-halogenation of some halo-organic compounds via hydrogen atom transfer processes [19]. However, silver and gold nanoparticle catalyzed HAAs degradation by BH_4^- has yet to be investigated thoroughly. It was therefore decided to study the de-halogenation of HAAs and their mechanism in more detail.

Sol-gel silica entrapped nanoparticles are one of the most extensively studied heterogeneous catalysts that have been successfully applied in several catalytic processes [20]. However, silica encapsulated noble metal nanoparticles have not been studied in waste water treatment, which motivated us to investigate gold and silver nanoparticles entrapped in silica sol-gel matrices in the present study. In this work, the origin of succinic acid as the key product of the debromination of tri-bromo-acetic acid has been successfully explained both experimentally and theoretically. DFT calculations indicate that the formation of succinic acid from (Au^0-NPs)-CX_2CO_2H increases along the series X = H, Cl, Br, I. The present study establishes that a variety of pathways are involved in the de-halogenation of halo-organic compounds. This study may forge new research directions in the field of noble metal nanoparticle catalyzed reductive dehalogenation processes.

2. Experimental section

2.1. Materials

Tri-bromo-acetic acid, di-bromo-acetic acid, mono-bromo-acetic acid, tri-chloro-acetic acid, tri-methoxymethylsilane, (3-aminopropyl)-trimethoxysilane, 2-bromo-propionic acid and 3-bromo-propionic acid were obtained from Alfa Aesar. Tetra-ethyl orthosilicate and gold(III) chloride tri-hydrate, silver nitrate, 2,3-di-bromo-propionic acid and $NaBD_4$ were purchased from Aldrich. $NaBH_4$ was bought from Strem Chemicals. All aqueous solutions were prepared from deionized water purified by a Millipore Milli-Q setup with a final resistivity of > 10 MΩ/cm.

2.2. Instrumentation and measurements

The surface areas of the blank matrix and of the catalysts were determined from N_2 adsorption-desorption isotherms measured at liquid nitrogen temperature using a NOVA 3200E Quantachrome analyzer. The specific surface area was calculated from the linear section of the Brunauer-Emmett-Teller (BET) plot.

The morphologies and compositions of the matrices were studied by scanning electron microscopy (Ultra-High Resolution Maia 3 FE-SEM) using an OXFORD EDS system for composition analysis with a X-Max 80 detector. The samples were prepared by dispersing the catalysts in water and placing one drop of the aqueous suspension onto a carbon tape. The tape was dried in air prior to the measurement. To determine the composition, energy dispersive X-ray analyses in SEM mode (SEM-EDX) were performed using the Aztec materials characterization system. XPS data were collected using an X-ray photoelectron spectrometer ESCALAB 250 ultrahigh vacuum (1×10^{-9} bar) apparatus with an AlK^{α} X-ray source and a monochromator. The X-ray beam size was 500 μm and survey spectra were recorded with pass energy (PE) 150 eV and high-energy resolution spectra were recorded with pass energy (PE) 20 eV. To correct for charging effects, all spectra were calibrated relative to a carbon C 1 s peak positioned at 284.8 eV. Processing of the XPS results was carried out using the AVANTAGE program. The metal loadings of the samples were measured on an Axios X-ray fluorescence (XRF) spectrometer. The method used for the XRF analysis is based on calibration curves obtained from standard samples for each element. De-halogenation of the halo-acetic acids was monitored by using an HPLC system (Jasco) with a UV/Vis detector (λ = 210 nm) along with an Agilent HPLC column (Eclipse XDB-C18, 5 μm) with dimensions of 4.6 × 150 mm. The eluent was H_2O/CH_3CN = 98:2 with 0.2% H_3PO_4, pH 2.0, and a flow rate of 1.0 mL min^{-1}. ^1H and ^{13}C NMR spectra (400 MHz and 100 MHz) were recorded on a Bruker Avance^{III} HD NMR spectrometer equipped with 5 mm BBO probe and Z-axis gradient coil. The samples were dissolved in H_2O and D_2O at 300 K using the residue of the solvent signal (4.79 ppm) as an internal standard. Long and short correlation between ^{13}C and ^1H (HMBC and HMQC) were done as needed.

2.3. Syntheses

Gold (**Au-cat**) and silver (**Ag-cat**) catalysts were prepared by using the two step acid/base sol-gel synthesis route as reported earlier [12]. Briefly, 6.0 mL of ice-cold water containing 90 μL of acid (HCl for Au-cat and HNO_3 for Ag-cat) was poured into a solution mixture consisting of 2.5 mL of Tri-methoxy-methyl-silane (MTMOS), 8.8 mL of Tetra-ethyl-ortho-silicate (TEOS) and 13.3 mL of ethanol. After stirring for 10 min, 125 μL of (3-aminopropyl)-tri-ethoxy-silane (APS) was added to the mixture, 5.0 mL of an ice cold aqueous solution of 3×10^{-3} M $HAuCl_4 \cdot 3H_2O$ was then added dropwise after which 5.0 mL of an aqueous solution of 3×10^{-2} M $NaBH_4$ was added for the reduction of Au (III). 5.0 mL of 2.8% NH_3 was then added for the conversion of the sol to gel. The final solution was stirred for several minutes to complete the gelation process. The solid gel was aged and dried for 7 days, after which the solid matrix (**Au-cat**) was washed several times with water. The washed matrix was dried, crushed with mortar and pestle into a powder and then used for the catalytic processes. **Ag-cat** was prepared following the same procedure as that used for **Au-cat** but with some modification, namely, the reduction of silver was not done immediately after the addition of silver nitrate but after ageing the gel matrix for one week.

2.4. Computational details

All calculations were carried out by using the Gaussian 09 suite of programs (Revision D.01) [21]. DFT calculations were performed with the M06 functional, which has been reported as reliable for reactions on Au nano clusters through several benchmark calculations [22]. The scalar relativistic effective core potential (ECP) with double-zeta basis sets [3s3p2d] (LANL2DZ) was used for the gold, chlorine, bromine and iodine atoms. This ECP treats the inner shell of gold (the Xe core) as an effective potential while it treats the 19 valence electrons in the outer shell (5s5p5d6s) explicitly. The 6-311 + G (d,p) basis set was used for the hydrogen, carbon, and oxygen atoms. We performed a fully relaxed structural optimization, and the unrestricted Kohn–Sham Scheme was employed for open-shell electronic structure calculations. All the ground-state optimized structures were local minima containing no imaginary frequencies, as confirmed by vibrational analysis.

2.5. Catalytic tests

All the catalytic reactions were performed by following the procedure reported previously [12a]. Briefly, 3.5 mL of a 0.010 M halo-organic acid was added to a suspension of 0.50 g of the catalyst in 18 mL of deionized water in a 50 mL beaker kept at room temperature. The mixture was then stirred for several minutes. Under fast addition,

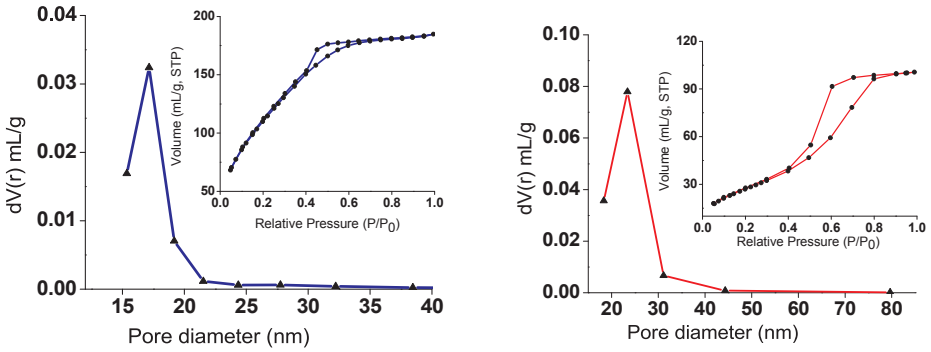

Fig. 1. (a) Barrett-Joyner-Halenda (BJH) pore size distribution of the Au-cat matrix, inset: Au-cat matrix nitrogen adsorption-desorption isotherm, (b) BJH pore size distribution of Ag-cat matrix, inset: Ag-cat matrix nitrogen adsorption-desorption isotherm.

3.5 mL of 0.060 M aqueous $NaBH_4$ (for **Au-cat**) or 0.020 M aqueous $NaBH_4$ (for **Ag-cat**) was then added in a single portion. The resulting suspension was stirred for 5 h. After completion of the reaction the catalyst was recovered by filtration and the filtrate was analyzed by HPLC. Isotopic labeling experiments were performed in a H_2O/D_2O medium and analyzed by NMR spectroscopy, where 20 times more substrate and reducing agent were used due to the lower sensitivity of NMR. The addition of $NaBH_4/NaBD_4$ was done in single portions in some experiments and slowly, dropwise, over a 5 h period in others. Each result reported is the average of at least three independent experiments. The error limit for the analytical results is ± 5%.

3. Results and discussions

3.1. Catalyst characterization

To gain insight into the pore systems of these materials, the nitrogen adsorption-desorption isotherms and the pore distributions of both the gold and silver catalysts were determined (Fig. 1). Both isotherms of the matrices could be classified as type IV curves that are characteristic of ordered meso-porous materials with uniform pores [23]. The Brunauer-Emmett-Teller (BET) surface area and pore volume of the Au-cat are 428 $m^2 g^{-1}$ and 0.286 $cm^3 g^{-1}$ (single point at $P/P_0 = 0.99448$), respectively, whereas the corresponding values for the Ag-cat are 452 $m^2 g^{-1}$ and 0.671 $cm^3 g^{-1}$ (single point at $P/P_0 = 0.98740$), respectively. Both catalysts have quite large surface areas and high inner porosities. However, the larger surface area and higher inner porosity motivates the substrates to be adsorbed more on the surface of the silver catalyst and followed by the easy diffusion of incoming reactants to the entrapped Ag^0-NPs, demonstrating the higher activity of the Ag-cat over the Au-cat (vide infra). The matrices have narrow BJH (Barrett-Joyner-Halenda) pore size distributions and the average BJH pore diameters are nearly 20 nm for both catalysts, suggesting that our synthesized materials exhibit meso-porosity.

The elements present on the surfaces of the catalysts and their oxidation states were examined by XPS analysis (Fig. 2). Typical full-scan spectra of the catalysts show Si, O and C in both catalysts. The binding energy for the C 1 s peak at 284.6 eV was used as the reference for calibration. The XPS spectra of oxygen (O 1 s) at 284.8 eV and silicone (Si 2 P) at 102.78 eV are from the silica matrices. The weak peaks of gold (Au 4f) and silver (Ag 3d) at 83.5 and 366.3 eV, respectively, demonstrate the zero-valent metallic nature of the Au^0 and Ag^0 present in the corresponding catalysts [24]. The weak nature of these metallic peaks clearly indicates that most of the nanoparticles are located in the inner pores of the matrices rather than on the catalyst surface. The XPS signals of the metallic gold and silver for both catalysts appear at significantly lower binding energies than those usually observed for the corresponding reference metallic states (84 eV for gold and 368 for silver) [25]. The presence of specific particle-support interactions was proposed to explain the negative shift in the binding energies [26].

XRF spectra of gold and silver present in their corresponding catalysts are presented in Fig. S1-2 (Supporting Information). The concentrations of the gold and silver nanoparticles obtained from the XRF spectrometer are well correlated with the quantities of nanoparticles contained in the matrices.

To understand catalyst morphology, scanning electron microscopy (SEM) images of the two catalysts and the blank matrix were taken (Fig. 3a, c and e). Energy-dispersive X-ray spectroscopy (EDX) was used with SEM to determine catalyst elemental compositions (Fig. 3b, d and f). From the SEM images, it can be concluded that the morphology did not change significantly after entrapment of the gold and silver nanoparticles. Very few white spots of gold and silver nanoparticle are observed in the SEM images, indicates that few nanoparticles are present on the surface and most of the nanoparticles are entrapped within the pores of the meso-porous material. EDX (inset images in Fig. 3d and f) spectra were obtained by focusing on the rare white dots observed on the surface. Major peaks for Si and O in EDX spectra obviously originate from the matrices. The very low weight percentages of gold and silver indicate good incorporation of the nanoparticles into the silica material. The absence of other peaks or the very low intensity peaks observed for other elements in the EDX spectroscopy results indicate relatively high catalyst purity.

3.2. Catalytic activities and mechanism

Previously reported results [12a] indicated that (a) succinic acid is a key product of the catalytic de-bromination of $Br_3CCO_2^-$ and $Br_2CHCO_2^-$ but not of $BrCH_2CO_2^-$ and (b) the rate of BH_4^- addition affected product distribution.

Since the formation of succinic acid requires the formation of a radical as an intermediate, it was proposed that the first steps in the de-bromination processes are [12a]:

$$(Au^0\text{-NP}) + nBH_4^- \rightarrow \{(Au^0\text{-NP})\text{-}H_{4n}\}^{-4n} + nB(OH)_3 \,/\, (BO_2\text{-} + H_3O^+) \quad (1)$$

Clearly this is a complex process, and some partially oxidized BH_4^- is formed as an intermediate. In aqueous solutions, this reaction is probably followed by:

$$\{(Au^0\text{-NP})\text{-}H_{4n}\}^{-4n} + mH_3O^+ \leftrightarrow \{(Au^0\text{ -NP})\text{-}H_{4n+m}\}^{(4n\text{-}m)\text{-}} + mH_2O \quad (2)$$

The equilibrium constant of reaction (2) depends on the pH of the solution. If the redox potential is below the over-potential for H_2 release from the Au^0-NPs, then reaction (2) will be followed by either:

$$\{(Au^0\text{-NP})\text{-}H_{4n+m}\}^{(4n-m)-} \rightarrow \{(Au^0\text{-NP})\text{-}H_{4n+m\text{-}2}\}^{(4n\text{-}m)\text{-}} + H_2 \quad (3)$$

or by:

$$\{(Au^0\text{-NP})\text{-}H_{4n+m}\}^{(4n-m)-} + H_3O^+/H_2O \rightarrow \{(Au^0\text{-NP})\text{-}H_{4n+m\text{-}1}\}^{(4n\text{-}m\text{-}1)\text{-}} + H_2 + H_2O/OH\text{-} \quad (4)$$

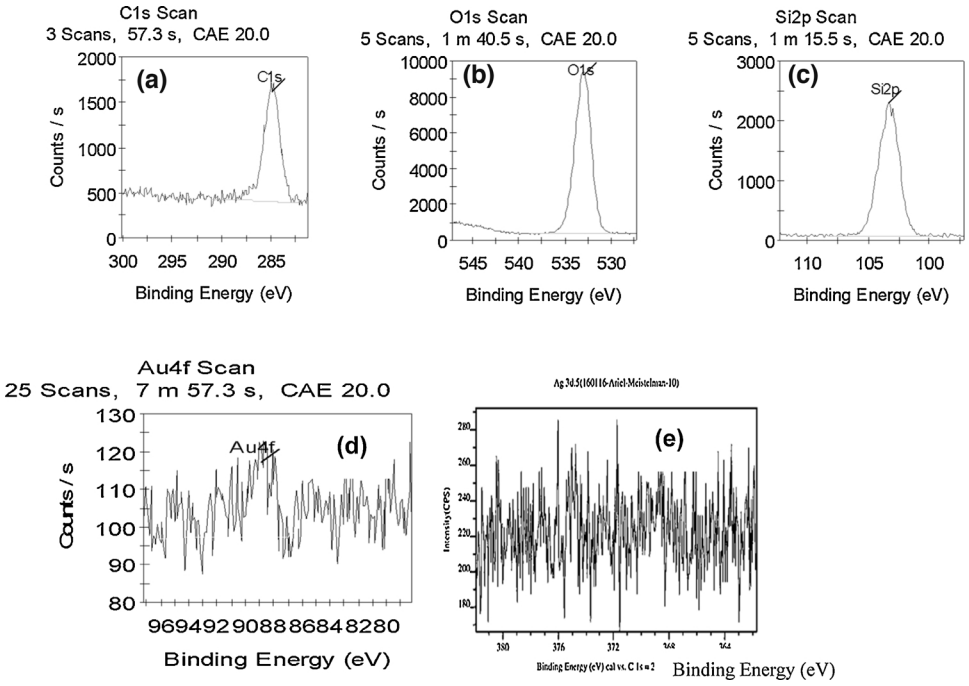

Fig. 2. XPS spectra of (a) C 1s, (b) O 1s, (c) Si 2p, (d) Au 4f for Au-cat and (e) Ag 3d for Ag-cat.

It should be noted that although H_2 is formed in these reactions, it does not react with halo-organic compounds directly, and it is thus proposed that the catalytic reductions by $\{(M^0\text{-NP})\text{-}H_{4n+m}\}^{(4n-m)-}$, e.g., of p-nitro-phenol, proceed via hydride transfer from the $\{(M^0\text{-NP})\text{-}H_{4n+m}\}^{(4n\text{-}m)\text{-}}$ [27].

In the presence of $CH_{3\text{-}k}Br_kCO_2H$, the $\{(Au^0\text{-NP})\text{-}H_{4n+m}\}^{m-4n}$ (from now on $\{(Au^0\text{-NP})\text{-}H_n\}^{m\text{-}}$) might react via one of the following mechanisms:

$$\{(Au^0\text{-NP})\text{-}H_n\}^{m-} + Br_kCH_{3\text{-}k}CO_2^- \rightarrow \{(Au^0\text{-NP})\text{-}H_n\}^{(m\text{-}1)\text{-}} + Br^- + Br_{k\text{-}1}CH_{3\text{-}k}CO_2^{\cdot -} \quad (5)$$

(k = 1;2;3), which is an electron transfer process, or:

$$\{(Au^0\text{-NP})\text{-}H_n\}^{m-} + Br_kCH_{3\text{-}k}CO_2^- \rightarrow \{(Au^0\text{-NP})\text{-}H_{n\text{-}1}\}^{m\text{-}} + Br^- + H^+ + Br_{k\text{-}1}CH_{3\text{-}k}CO_2^{\cdot -} \quad (6)$$

a hydrogen atom transfer process, followed by the reaction of the radical with the substrate to form the M—C bond:

$$\{(Au^0\text{-NP})\text{-}H_n\}^{(m-1)\text{-}} + Br_{k\text{-}1}CH_{3\text{-}k}CO_2^{\cdot -} \rightarrow \{(Au^0\text{-NP})\text{-}H_n\}\text{-}CBr_{k\text{-}1}H_{3\text{-}k}CO_2^{\,m-} \quad (7)$$

Reaction (7) is expected to be very fast, as all alkyl radicals react with M^0-NPs in reactions that approach the diffusion-controlled limit [28]. The succinic acid is probably formed via migration of the $-CBr_2CO_2^-$ and/or the $-CBrHCO_2^-$ on the surfaces of the Au^0-NPs in a manner analogous to the migration of methyl radicals on the surfaces of the Au^0-NPs [14i,28d,29]. Alternatively, the succinic acid may be formed in the homogeneous solution after homolysis of the Au—C bond. Therefore, the fact that succinic acid is not obtained in the reduction of $BrCH_2CO_2^-$ indicates that the transients $[\{(Au^0\text{-NP})\text{-}H_n\}\text{-}CBr_2CO_2]^{m\text{-}}$ and $[\{(Au^0\text{-NP})\text{-}H_n\}\text{-}CBrHCO_2]^{m\text{-}}$ have chemical properties that are significantly different from those of $[\{(Au^0\text{-NP})\text{-}H_n\} - CH_2CO_2]^{m\text{-}}$ [12a].

Since bromine substituents are stronger electron withdrawing groups than hydrogen atoms, it was first assumed that this is the source of the observed differences in the reduction mechanisms ($Br_3CCO_2^-$ and $Br_2CHCO_2^-$ produce succinic acid whereas $BrCH_2CO_2^-$ generates acetic acid). To assess this possibility, the de-chlorination of $Cl_3CCO_2^-$ was studied [12a], but because no succinic acid was formed, this explanation can be ruled out. Another plausible source of the observed results is the steric effect of the groups attached to the α-carbon atom bound to the gold nanoparticle, since bromine is considerably larger than chlorine or hydrogen. To determine whether this is the case, we studied the de-bromination reactions of 2-bromo-propionic-acid (2-BPA), 3-bromo-propionic-acid (3-BPA) and 2,3-di-bromo-propionic-acid (2,3-DBPA). The reductions of these substituted propionic acids using aqueous $NaBH_4$ were performed using the same procedure used for tri-bromo-acetic acid (TBAA) and TCAA [12a]. The results are summarized in Fig. 4. Surprisingly, no succinic acid derivatives are observed as one of the products in any of these systems.

The de-bromination of 2-BPA under our experimental conditions yielded 90% propionic acid (PA) while the rest was unreacted 2-BPA. In contrast, 3-BPA was found to be more difficult to reduce under our catalytic conditions and only 24% of PA was formed and 76% 3-BPA remained unreacted. The latter observation is in accordance with the known C—Br bond strengths in 2-BPA and 3-BPA, wherein those of the former are considerably weaker due to the resonance stabilization of the radical $C(CH_3)HCO_2H\cdot$ and more so for the $C(CH_3)HCO_2^-$ radical. On the other hand, 66.7% acrylic acid and 6.5% 2-BPA were formed during the catalytic de-bromination of 2,3-DBPA (Fig. 4). The observation that acrylic acid is the main product is further proof that the primary radicals formed bind to the Au^0—NPs, as halide β-elimination processes occur only when the primary radical forms a σ bond to a metal complex [30] or to a metal surface [14i–j]. Surprisingly, the products consist of 6.5% 2-BPA but no 3-BPA. This is unexpected, since the rate of 2-BPA reduction is considerably higher than that of 3-BPA. One possible explanation of this result is that the transients formed in these reductions, $[\{(Au^0\text{-NP})\text{-}H_n\}\text{-}CH(CH_2Br)CO_2]^{m-}$ and $[\{(Au^0\text{-NP})\text{-}H_n\}\text{-}CH_2CHBrCO_2]^{m-}$, respectively, decompose via different routes.

$$\begin{array}{ll} \text{(a)} & \rightarrow \{(Au^0\text{-NP})\text{-}H_n\}^{(m\text{-}1)\text{-}} + CH_2{=}CHCO_2^- + Br^- + H^+ \\ [\{(Au^0\text{-NP})\text{-}H_n\}\text{-}CH(CH_2Br)CO_2]^{m\text{-}} & \xrightarrow{H^+} \\ \text{(b)} & \rightarrow \{(Au^0\text{-NP})\text{-}H_n\}^{(m\text{-}2)\text{-}} + CH_2(CH_2Br)CO_2^- \end{array} \quad (8)$$

$$\begin{array}{ll} \text{(a)} & \rightarrow \{(Au^0\text{-NP})\text{-}H_n\}^{(m\text{-}1)\text{-}} + CH_2{=}CHCO_2^- + Br^- + H^+ \\ [\{(Au^0\text{-NP})\text{-}H_n\}\text{-}CH_2CHBrCO_2]^{m\text{-}} & \xrightarrow{H^+} \\ \text{(b)} & \rightarrow \{(Au^0\text{-NP})\text{-}H_n\}^{(m\text{-}2)\text{-}} + CH_3CHBrCO_2^- \end{array} \quad (9)$$

The results indicate that $k_{8a} >> k_{8b}$, and therefore, no 3-BPA was observed in the products. In contrast, $k_{9b} \geq k_{9a}$, and consequently, some 2-BPA was obtained. The source of the differences in their reactivity is not clear at the moment.

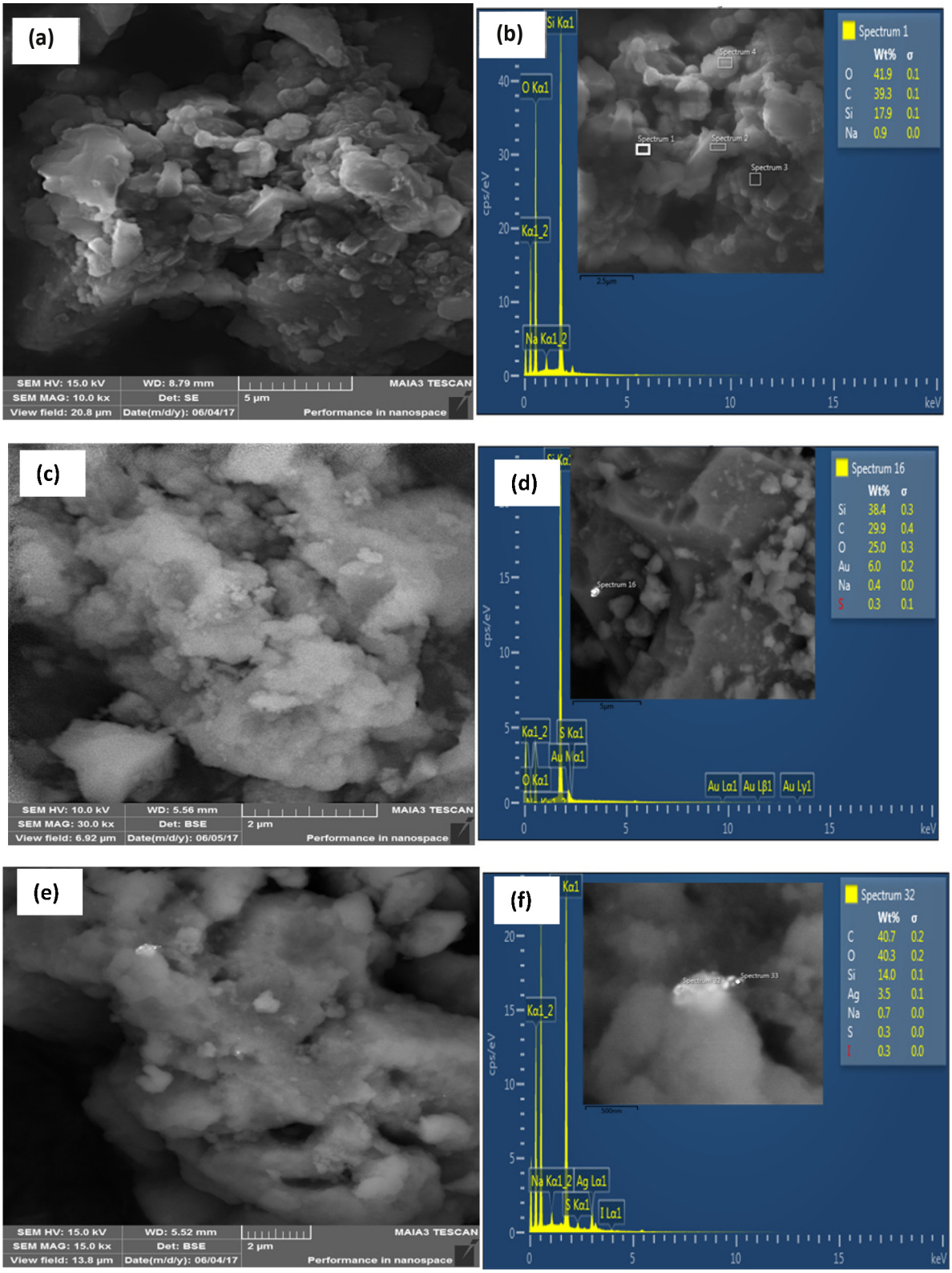

Fig. 3. Scanning electron microscope images of (a) blank matrix, (c) Au-cat and (e) Ag-cat. Energy-dispersive X-ray spectroscopy (EDX) spectra of (b) blank matrix, Au-cat (d) and Ag-cat (f).

However, the major conclusion of these experiments is that neither the electron withdrawing properties nor the steric effects can explain the origin of succinic acid formation. Thus, the origin of this process seems to be some electronic interaction between the non-bonding p-electrons of the bromine atom with the Au—C σ bond, which would weaken it and either enable the migration of the $–CBr_2CO_2^-$/ $–CHBrCO_2^-$ on the surface, leading to dimerization, or to the release of $CBr_2CO_2^{\cdot-}$/$CHBrCO_2^{\cdot-}$ radicals into the solution. The latter possibility is ruled out, as these radicals will probably react with the BH_4^- present in the solution [31]. Furthermore, the reaction of the $CBr_2CO_2^{\cdot-}$/

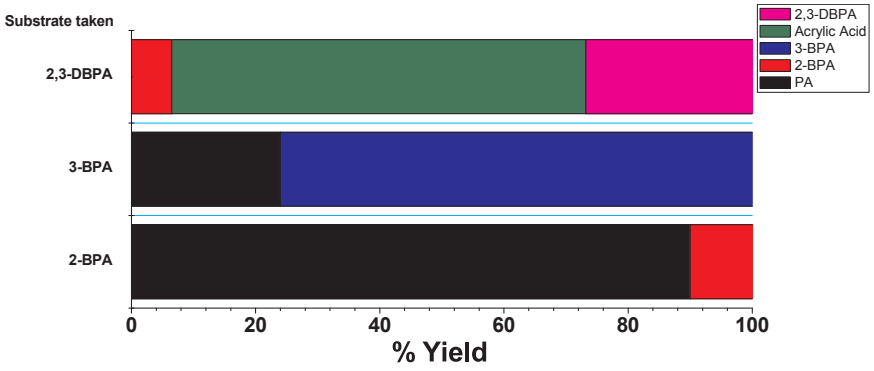

Fig. 4. Au-cat catalyzed reduction of 2-bromo-propionic-acid (2-BPA), 3-bromo-propionic- acid (3-BPA) and 2,3-di-bromo-propionic-acid (2,3-DBPA). [Substrate] = 1.4×10^{-3} M, [BH_4-] = 8.4×10^{-3} M. $NaBH_4$ was added in one portion, fast addition. pH ≈.6.5–7.5.

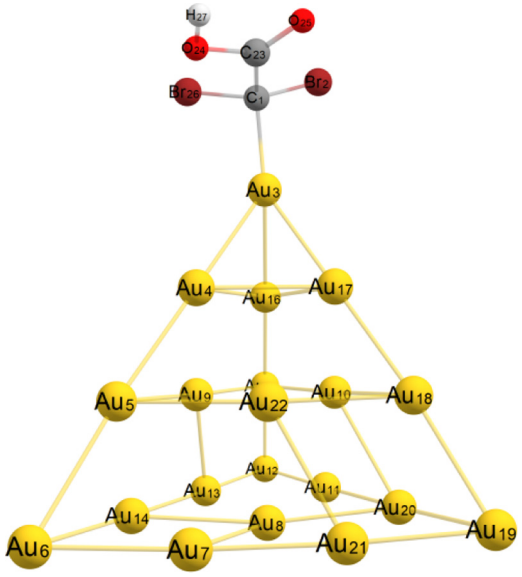

Fig. 5. Optimized geometry of Au_{20}^0–CBr_2CO_2H (DBA-Au_{20}^0).

$CHBrCO_2^{\cdot-}$ radicals with BH_4- would yield products that contain hydrogens that stem from BH_4^- and not from the solvent, but this was also ruled out below. Computational calculations of the bond strengths of Au-C σ bonds were done to test this assumption. The Au_{20} nanocluster was chosen for these calculations as it was used in previous studies on methanol oxidation and on the aerobic homocoupling of phenylboronic acid [32,33]. Then the $–CX_2CO_2H$ fragment (X = H, Cl, Br or I) was bound to the Au_{20} cluster at the atom at the apex of the cluster. The $–CX_2CO_2H$ was chosen as it is formed in the de-halogenations of CH_2BrCO_2H, CCl_3CO_2H and CBr_3CO_2H, respectively.

Table 1
Wiberg indexes and bond lengths for Au—C σ bond.

Species	Au-C	Wiberg index	Bond length (Å)
$HOOCCH_2$-Au_{20}^0	Au3 – C1	0.4797	2.158
$HOOCCCl_2$-Au_{20}^0	Au3-C1	0.3794	2.164
$HOOCCBr_2$-Au_{20}^0	Au3-C1	0.3687	2.164
$HOOCCI_2$-Au_{20}^0	Au3-C1	0.3579	2.167

Clearly the properties of the apex Au atom differ from those of the other Au atoms, but this can be said for any Au atom chosen. It is reasonable to assume that the relative Au—C bond lengths and bond energies are similar for all the Au atoms in Au^0-NPs. The optimized structure for $HOOCCBr_2$-Au_{20}^0 (DBA-Au_{20}^0) is depicted in Fig. 5, and the remaining optimized structures are shown in the supporting information file. All the structures exhibit very similar geometries, selected bond lengths of which are listed in Table S1 (Supporting Information). The slight differences observed in those structures are due to differences in electronegativity and van der Waals radii between the hydrogen and the halogen atoms. The results based on NBO analysis are presented Table 1. The results for both the Wiberg index [34], which provides bond order, and the Au—C bond lengths clearly point out that the bond strength of $HOOCCBr_2$-Au_{20}^0 is weaker than that of $HOOCCCl_2$-Au_{20}^0 and $HOOCCH_2$-Au_{20}^0. Therefore, the results indicate that it is reasonable that the $–CBr_2CO_2H$ fragment will migrate more freely on the surface of the Au^0-NPs than will either the $–CCl_2CO_2H$ or the $–CH_2CO_2H$ fragment. Such migration enables the dimerization of the $–CBr_2CO_2H$ fragments and leads to the formation of succinic acid via reaction (10).

$$\{(Au^0\text{-NP})\text{-}H_n\}\text{-}(CBr_{k\text{-}1}H_{3\text{-}k}CO_2)_l^{(m+1-1)-} \rightarrow \{(Au^0\text{-NP})\text{-}H_n\}\text{-}(CBr_{k\text{-}1}H_{3\text{-}k}CO_2)_{l\text{-}2}^{(m+1\text{-}3)\text{-}} + (\text{-}CBr_{k\text{-}1}H_{3\text{-}k}CO_2)_2^{2-} \quad (10)$$

Reaction (10) will be followed by the de-bromination of the product to yield succinic acid.

$$\{(Au^0\text{-NP})\text{-}H_n\}\text{-}(CH_2CO_2)_l^{(m+1-1)-} \rightarrow \{(Au^0\text{-NP})\text{-}H_{n\text{-}1}\}\text{-}(CH_2CO_2)_{l\text{-}1}^{(m+1\text{-}2)\text{-}} + CH_3CO_2\text{-} \quad (11)$$

In principle, the final products, acetic acid and succinic acid, may be formed via one of the following reactions (for simplicity, the equations are only written out for acetic acid):

$$\{(Au^0\text{-NP})\text{-}H_n\}\text{-}(CH_2CO_2)_l^{(m+1-1)-} + H^+ \rightarrow \{(Au^0\text{-NP})\text{-}H_n\}\text{-}(CH_2CO_2)_{l\text{-}1}^{(m+1\text{-}3)\text{-}} + CH_3CO_2\text{-} \quad (12)$$

This reaction involves the migration of one H atom on the surface to the M^0-$CR^1R^2R^3$ group leading to the formation of H-$CR^1R^2R^3$. This

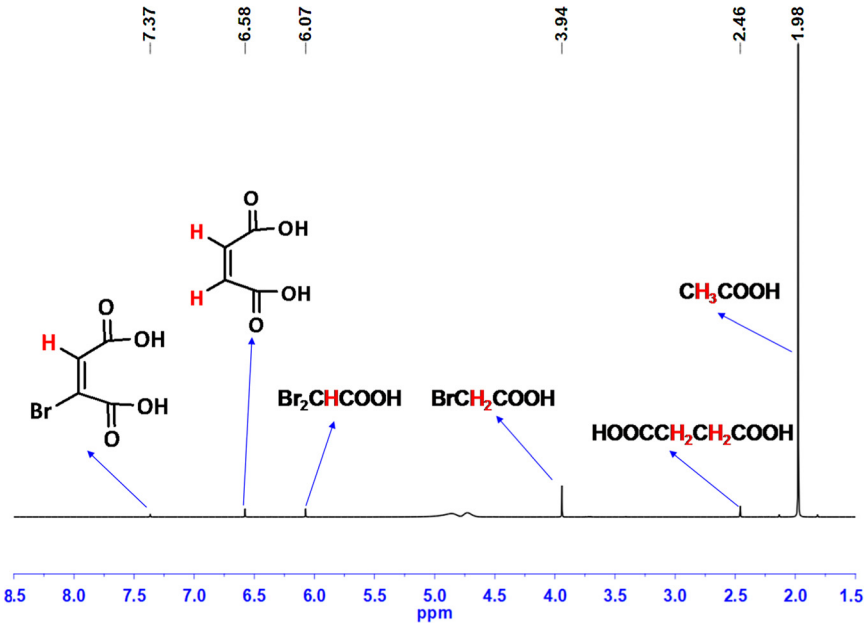

Fig. 6. ^{1}H-NMR of the products obtained in tri-bromo-acetic acid reduction by $NaBH_4$ catalyzed by gold nanoparticles in H_2O as the solvent. [TBAA] = 2.8×10^{-2} M, [BH_4-] = 16.8×10^{-2} M. $NaBH_4$ was added in one portion, fast addition. pH ≈.6.5–7.5.

reaction is analogous to the Tafel mechanism [35,36].

In this mechanism, one H^+ from the solution attacks the carbon atom bound to the nanoparticle in a reaction analogous to the Heyrovsky mechanism [35,36].

$$\{(Au^0\text{-NP})\text{-}H_n\}\text{-}(CH_2CO_2)_l^{(m+1-1)-} + CH_2CO_2\cdot\text{-} \rightarrow \{(Au^0\text{-NP})\text{-}H_{n-1}\}\text{-}(CH_2CO_2)_l^{(m+1-1)-} + CH_3CO_2\text{-} \quad (13)$$

Here, a carbon-centered radical attacks the carbon atom bound to the nanoparticle. Analogous reactions were reported for complexes with M—C bonds in aqueous solution [37].

$$CH_2CO_2^{\cdot -} + BH_4\text{-} \rightarrow CH_3CO_2\text{-} + BH_3^{\cdot -}/BH_4\cdot \quad (14)$$

Although reaction (14) was already ruled out above as a significant contributing mechanism, some of the final products could still have been formed via this reaction. In reactions (11) and (13), the source of the hydrogen atoms is the $\{(Au^0\text{-NP})\text{-}H_n\}^{m-}$ nanoparticles, whereas if reaction (12) is the major route, then the source of the hydrogen atoms is the solvent. Even if reaction (2) contributes significantly, i.e. a large part (though less than 50%) of the hydrogen atoms on the nanoparticle stem from the solvent, the product (acetic acid) is expected to contain hydrogen atoms that stem from the BH_4-.

It was therefore decided to use isotopic labeling to identify the source of the hydrogens in the acetic and succinic acids formed in the catalyzed de-bromination of TBAA on the Au-cat. These experiments are based on the observation that the isotopic exchanges between $\{(Au^0\text{-NP})\text{-}H_{4n+m}\}^{m-4n}$ and the water solvent and between BD_4- and water are considerably slower than reactions (3) and/or (4) [38]. Three different isotopic compositions were chosen: (i) $NaBH_4/H_2O$, (ii) $NaBD_4/H_2O$ and (iii) $NaBH_4/D_2O$. The product yields were then monitored

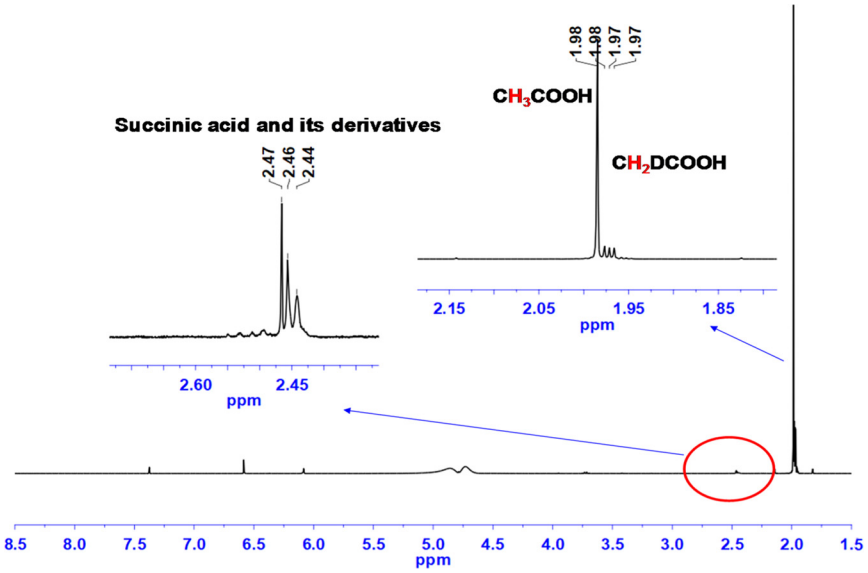

Fig. 7. ^{1}H-NMR of the products obtained in tri-bromo-acetic-acid reduction by $NaBD_4$ catalyzed by gold nanoparticles in H_2O as the solvent. Inset: Zoom of the peaks at 1.95 and 2.45 ppm. [TBAA] = 2.8×10^{-2} M, [BD_4-] = 16.8×10^{-2} M. $NaBH_4$ was added in one portion, fast addition. pH ≈.6.5–7.5.

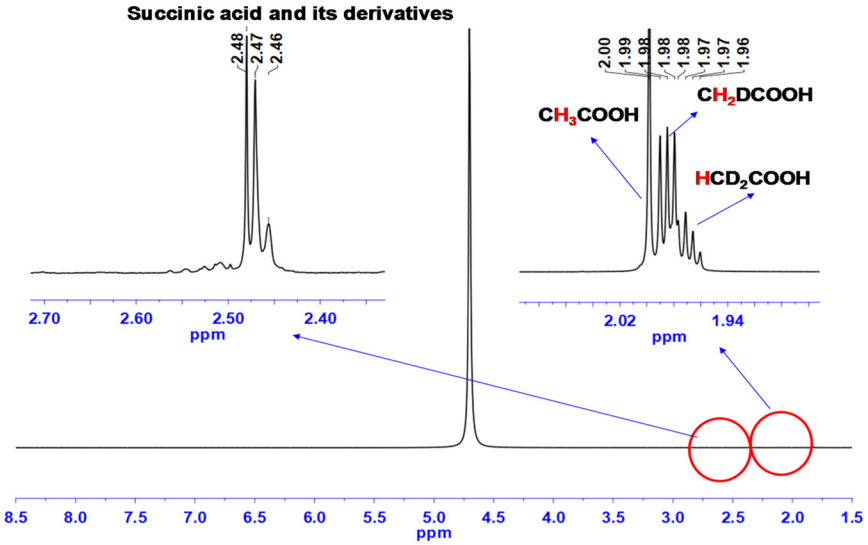

Fig. 8. ^{1}H-NMR of the products obtained in tri-bromo-acetic-acid reduction by $NaBH_4$ catalyzed by gold nanoparticles in D_2O as a solvent. Inset: Zoom of the peaks at 1.95 and 2.45 ppm. [TBAA] = 2.8×10^{-2} M, [BH_4-] = 16.8×10^{-2} M. $NaBH_4$ was added in one portion, fast addition. pH ≈ 6.5–7.5.

using NMR analysis. Due to the lower sensitivity of the NMR analysis, higher concentrations (20 times higher) of both substrates and of BH_4-/BD_4- were used in these experiments. This is expected to affect the product distributions due to the change in [BH_4-], which was shown to affect product compositions [12a], probably mainly due to a change in the redox potential of the $\{(Au^0\text{-NP})\text{-}H_n\}\text{-}(CBr_{k\text{-}1}H_{3\text{-}k}CO_2)_l^{(m+l\text{-}1)\text{-}}$ and/or due to the larger negative charge on the nanoparticles. A major acetate peak along with the moderate intensity peaks of other products are observed in the ^{1}H-NMR of the first two experiments (Figs. 6 and 7). However, these peaks become almost negligible in intensity when D_2O is used as the solvent, (Fig. 8). This finding is in accord with the previous report that the relative yields of succinic acid and acetate decreases with the increase in the rate of addition of BH_4- [12a]. These results clearly indicate that virtually all the hydrogen atoms in the products originated from the solvent and not from the borohydride, i.e., via reaction (12). The observation is that some CH_3CO_2- was formed in D_2O (Fig. 8) clearly shows that, more than statistically possible, some hydrogen atoms stem from the borohydride, i.e., the products are formed via two mechanisms, one major and the other minor. This outcome may be due to one of two reasons: (a) the hydrogens stemming from BH_4- appear mainly when the steady state concentration of BH_4- decreases, (see below), as its concentration always decreases at the end of the process, or, (b) the existence of different sites on the nanoparticles with different Au^0—C and/or Au^0—H bond strengths. An analogous situation was recently reported for Pt^0—C bonds [39]. Enlargement of the NMR spectrum demonstrates a splitting of the ^{1}H-NMR signals, which signifies that the hydrogens in the molecule are in close proximity to the deuterium atoms (Fig. 8).

The two peaks (Fig. 6**)** in the higher chemical shift region (δ 6.6 and δ 7.4), assigned to fumaric/maleic acid and/or their bromo derivatives, were only obtained in the reaction of TBAA. The absence of these peaks in the case of TCAA (vide infra) clearly supports the dimerization of the intermediates via reaction (10) followed by a β-elimination analogous to reaction (8), which only takes place in the case of TBAA. ^{13}C-NMR spectra for all the aforementioned three reactions are depicted in Figs. S3-5 (Supporting Information file). The ^{13}C-NMR (Fig. S5) of the last reaction mixture contains split spectra with high intensities for acetate and succinate, demonstrating the high abundance of deuterium in the acetic acid and the succinic acid obtained as products.

The three isotopic experiments were also performed with the slow addition (for 5 h) of the reducing agents ($NaBH_4$/$NaBD_4$) to the reaction mixture to assess the effects of its mode of addition on product distribution. NMR spectra of the corresponding reactions are reported in Figs. S6-11 (Supporting Information file). The results seem to contradict our previous report, where succinic acid was the main product when the reducing agent was added slowly [12a]. However, as mentioned above, 20 times higher concentrations of both the substrate and the reducing agent were used for the runs using NMR analysis in comparison to the reactions performed for HPLC analysis in the presence of the same amount of catalyst. Thus, although the reducing agent was added slowly, the reaction passed through a steady state similar to that obtained for the reaction in which the reducing agent was added in one portion (fast addition). Therefore, acetic acid was the main product. Nevertheless, the NMR study also suggests that during “slow” addition, more hydrogens in the products stemmed from the reducing agent than was found in the fast addition procedure. The CH_3COOH: CDH_2COOH:

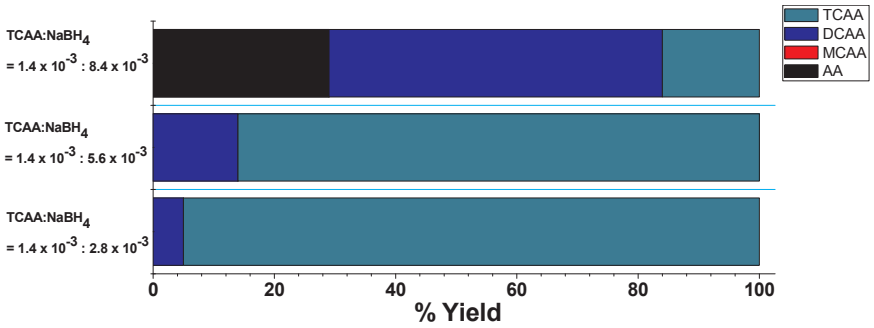

Fig. 9. Au-cat catalyzed TCAA reduction at different [TCAA]/[$NaBH_4$] molar ratios. $NaBH_4$ was added in one portion, fast addition. pH ≈.6.5–7.5.

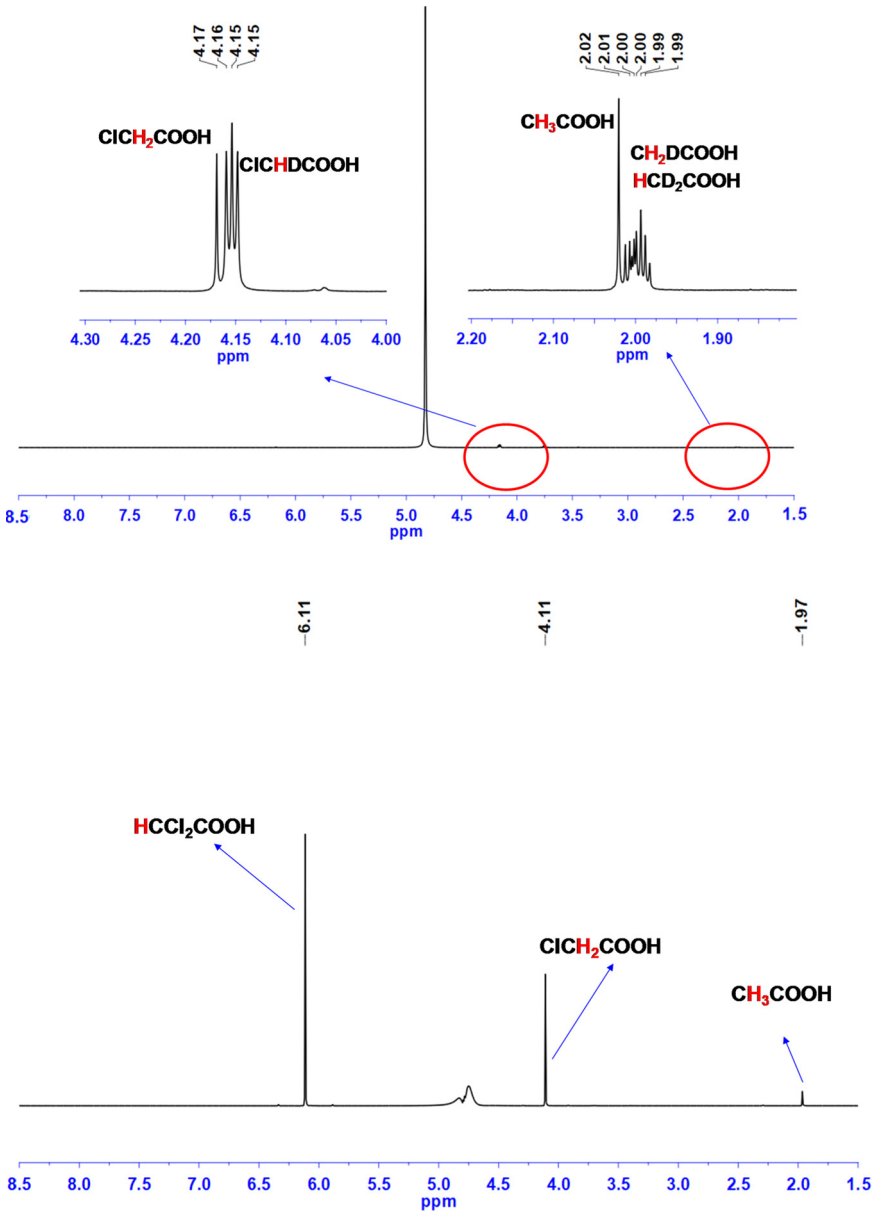

Fig. 10. ^{1}H-NMR of the products obtained in tri-chloro-acetic acid reduction catalyzed by gold nanoparticles in the presence of (i) $NaBH_4/D_2O$ (top) or (ii) $NaBD_4/H_2O$ (bottom). Inset: Zoom of the peaks at 1.95 and 4.0 ppm. [TCAA] = 2.8×10^{-2} M, [BH_4-] = 16.8×10^{-2} M. $NaBH_4$ was added in one portion, fast addition. pH ≈.6.5–7.5.

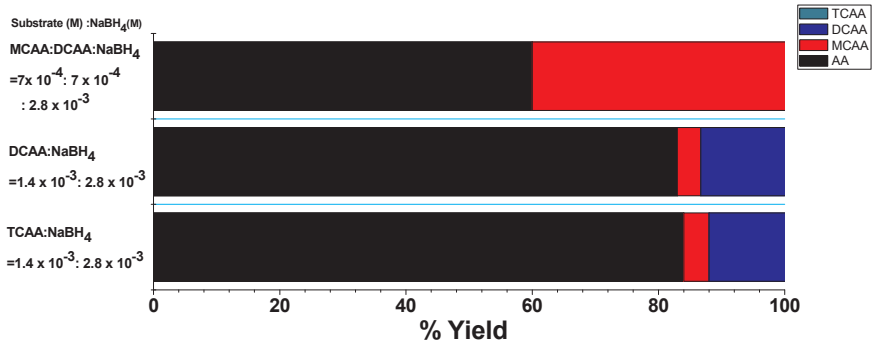

Fig. 11. Ag-cat catalyzed TCAA, DCAA and MCAA de-chlorination. $NaBH_4$ was added in one portion, fast addition. pH ≈.6.5–7.5.

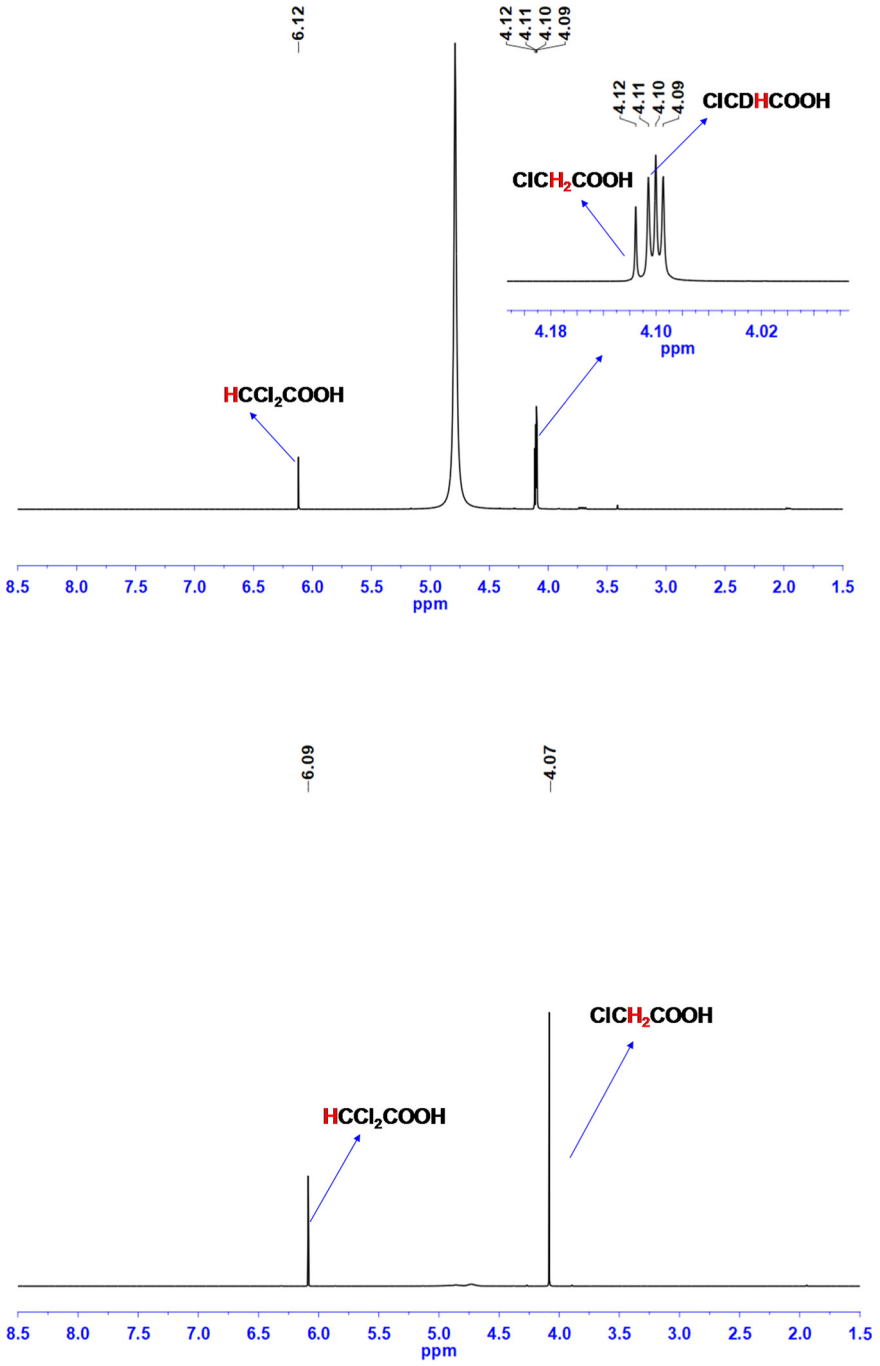

Fig. 12. ^{1}H-NMR of the products obtained in di-chloro-acetic acid reduction catalyzed by silver nanoparticle in the presence of (i) $NaBH_4$/ D_2O (top) and (ii) $NaBD_4$/ H_2O (bottom). Inset: Zoom of the peak at 4.1 ppm. [DCAA] = 2.8×10^{-2} M, [BH_4-/BD_4-] = 5.6×10^{-2} M. $NaBH_4$ was added in one portion, fast addition. pH ≈.6.5–7.5.

CD_2HCOOH ratio obtained in the fast addition of $NaBD_4$ was 1: 0.3: 0.1, whereas in the slow addition the ratio became 1: 1.1: 1.5. Clearly the ^{1}H NMR does not detect CD_3COOH.

The results also reveal that the succinic acid is not formed via the homogeneous reaction, thus confirming that the mechanism of TBAA de-bromination is a stepwise process, in which DBAA and MBAA, and finally AA, are formed. Moreover, the results support the formation of succinic acid via the dimerization of $–CBr_2CO_2^-$ and/or of $–CBrHCO_2^-$ on the surface of the Au^0-NPs [12a].

Au-cat catalyzed TCAA de-chlorination was studied by varying the mole ratio of TCAA to $NaBH_4$ from 1:2 to 1:6. Almost no degradation of TCAA was found at the lowest concentration of the reducing agent ([TCAA]:[$NaBH_4$] = 1:2). Even at a 1:4 ratio, only 14% of TCAA was converted to DCAA and the rest was unreacted. 29% AA, 55% DCAA were formed and a remaining 16% TCAA was undisturbed at a 1:6 ratio, (Fig. 9). The differences between TBAA de-bromination and TCAA de-chlorination stem from the stronger bond strength of C—Cl compared to that of C—Br. This requires that the Au^0-NP be reduced by the addition of more hydrides prior to the start of the de-halogenation process. As a result, the contributions of reactions (3) and (4) are larger while the yield of the de-halogenation is smaller.

Surprisingly, here no MCAA was formed though some AA was formed. This interesting phenomenon implies that the sol-gel entrapped gold nanoparticles catalyze the reductive de-halogenation via a

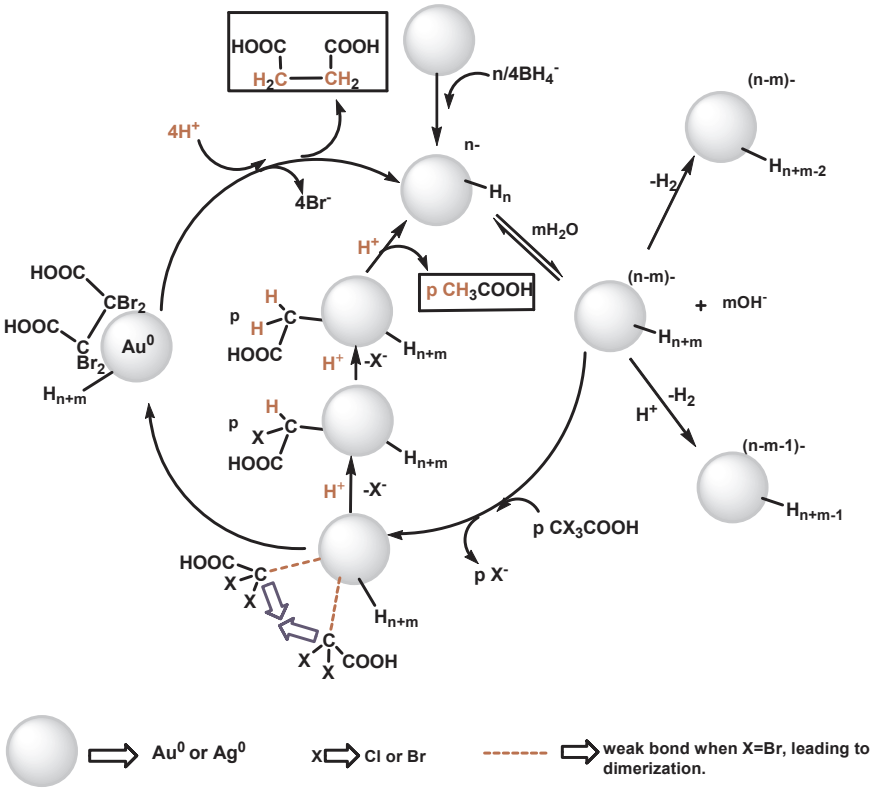

Scheme 1. Schematic diagram of the production of the two main products, acetic acid (for $Cl_3CCO_2^-$) and succinic acid (for $Br_3CCO_2^-$). Hydrogens in the reduced species originate mainly from the solvent water.

different mechanism. However, MCAA generation in the stepwise reduction of TCAA to AA has been reported in the literature [13]. Au-cat catalyzed TCAA reduction was also investigated using the isotope labeling method (Fig. 10). We performed two analogous reactions wherein Au-cat catalyzed TCAA reduction was studied in the presence of (i) $NaBH_4/D_2O$ or (ii) $NaBD_4/H_2O$. The ^{1}H-NMR peaks of the products of the first reaction are difficult to see. However, zooming in on the relevant regions reveals the peaks for acetic acid and its deuterated derivatives at nearly δ 2.0 ppm and those for mono-chloro-acetic acid and its deuterated derivative at around δ 4.0 ppm (Fig. 10). The fact that mono-chloro-acetic acid is obtained in the isotopic labeling experiment and not in the regular catalytic experiments is due to the higher concentrations of the reactants used in the former, which affects the concentrations of both hydrogen and the halogenated intermediates on the surface of the nanoparticle, thus resulting in a different product distribution. In the ^{13}C-NMR of this reaction, one can easily observe the corresponding peaks without zooming in, suggesting that fully deuterated compounds are present in copious amounts (Fig. S12, Supporting Information). In the second reaction, the peaks are easily recognizable, even without enlargement, signifying the presence of hydrogenated compounds. From this study, one can also conclude that for Au-cat catalyzed TCAA reduction, the hydrogens originate mainly from the solvent water, as was already proposed for TBAA reduction (vide supra).

It seemed of interest to compare the properties of the Au^0-NPs and Ag^0-NPs as catalysts for the de-halogenation processes studied. Therefore, Ag-cat was used to study the reductive de-halogenation of TBAA and TCAA. In the case of TBAA, AA was the major product (87%) while the yield of SA was only 13%. The major difference in the analogous result for the same reaction with Au-cat [12a] shows that the competition between the following reactions:

$$\{(M^0\text{-NP})\text{-}H_n\}\text{-}(CX_{k\text{-}1}H_{3\text{-}k}CO_2)_l^{(m+1-1)-} \rightarrow \{(M^0\text{-NP})\text{-}H_n\}\text{-}(CX_{k\text{-}1}H_{3\text{-}k}CO_2)_{l\text{-}2}^{(m+1\text{-}3)\text{-}} + (\text{-}CX_{k\text{-}1}H_{3\text{-}k}CO_2)_2^{2\text{-}}\ X = Cl \text{ or } Br \quad (15)$$

$$\{(M^0\text{-NP})\text{-}H_n\}\text{-}(CX_{k\text{-}1}H_{3\text{-}k}CO_2)_l^{(m+1-1)-} + H^+ \rightarrow \{(M^0\text{-NP})\text{-}H_n\}\text{-}(CX_{k\text{-}1}H_{3\text{-}k}CO_2)_{l\text{-}1}^{(m+1\text{-}3)\text{-}} + CX_{k\text{-}1}H_{4\text{-}k}CO_2\text{-}\ X = Cl \text{ or } Br \quad (16)$$

depends dramatically on the nature of M^0. This is not surprising, as clearly the M^0—C bond strengths of the different metals differ considerably.

Another interesting result is that TCAA is totally degraded into 84% AA, 12% DCAA and only 4% of MCAA at only a 1:2 M ratio of TCAA to $NaBH_4$ (Fig. 11). This is considerably more efficient than the same process catalyzed by Au^0-NPs (Fig. 9). The Ag-cat process also yields a very small amount of MCAA. This means that although both silver and gold nanoparticles catalyze the reductive de-chlorination of TCAA, these processes do not follow the conventional step-wise pathway of degradation that often ends in the formation of mono-chloro-acetic-acid [40]. To confirm this conclusion, DCAA degradation was studied. The results obtained for Ag-cat are very similar to those obtained for the TCAA reduction, which implies that the two processes proceed via analogous mechanisms (Fig. 11). To elucidate the origin of the AA, the de-chlorination of a 1:1 mixture of DCAA and MCAA via the catalytic process was studied. The product distribution, with 60% AA and 40% MCAA, indicates that 50% of the AA was originated from DCAA while only 10% AA was produced from MCAA. This result confirms that little

MCAA is formed as an intermediate in the catalytic de-chlorinations of TCAA and DCAA on Ag^0-NPs. Ag-cat catalyzed DCAA reduction was also scrutinized isotopically (Fig. 12). In this case, the results also indicate that the hydrogens in the products stem from the solvent. Therefore, the mechanism of de-chlorination of DCAA is probably:

$$\{(Ag^0\text{-NP})\text{-}H_n\}^{m-} + Cl_2CHCO_2^- \rightarrow \{(Ag^0\text{-NP})\text{-}H_{n-1}\}^{m-} + Cl^- + H^+ + ClCHCO_2^{\cdot -} \quad (17)$$

$$\{(Ag^0\text{-NP})\text{-}H_{n-1}\}^{m-} + ClCHCO_2^{\cdot -} \rightarrow \{(Ag^0\text{-NP})\text{-}H_{n-1}\}\text{-}CHClCO_2^{(m+1)-} \quad (18)$$

$$\{(Ag^0\text{-NP})\text{-}H_{n-1}\}\text{-}CHClCO_2^{(m+1)-} \rightarrow \{(Ag^0\text{-NP})\text{-}H_{n-1}\}\text{-}C\text{-}\delta HCO_2^{m-} + Cl^- \quad (19)$$

$$\{(Ag^0\text{-NP})\text{-}H_{n-1}\}\text{-}C^{-\delta}HCO_2^{m-} + H_2O \rightarrow \{(Ag^0\text{-NP})\text{-}H_{n-1}\}\text{-}CH_2CO_2^{(m-1)-} + OH^- \quad (20)$$

$$\{(Ag^0\text{-NP})\text{-}H_{n-1}\}\text{-}CH_2CO_2^{(m-1)-} + H_2O \rightarrow \{(Ag^0\text{-NP})\text{-}H_{n-1}\}^{(m-3)-} + CH_3CO_2^- + OH^- \quad (21)$$

All the above reactions represent the reduction of tri-chloro-acetic acid to acetic acid on the nanoparticle surfaces and not through the formation of mono-chloro-acetic acid.

Based on all the results obtained here and on the DFT calculations, we propose a plausible mechanistic pathway for HAA de-halogenation (Scheme 1).

The reusability of both the catalysts was reported in our previous publication [12]. However, reusability tests of the gold catalyst were repeated for 2-bromopropionic acid (Fig. S13, Supporting Information). Catalyst characterization after the catalytic test clearly demonstrated that both the catalysts remained stable, even after several cycles.

4. Concluding remarks

In summary, easy synthesis procedures for sol-gel entrapped gold and silver nanoparticles were developed. Our synthesized heterogeneous catalysts exhibit potent activity towards the reductive de-halogenation of tri-bromo and tri-chloro acetic acids. The results showed unexpectedly that the detailed mechanisms of the catalytic reductive de-halogenation reactions of TCAA and TBAA differ from each other. Moreover, our findings also show that the two reactions depend on the nature of the M^0 and on the rate of addition of the reducing agent. The source of most of the hydrogen atoms in the products was the solvent water. However, when the reducing agent was added slowly, the products contained more hydrogens that stem from BH_4^-. This clearly suggests that the decomposition of the (M^0—NP) —C bond proceeds via a Heyrovsky-like mechanism in the presence of high steady state concentrations of the reducing agent [35,36]. On the other hand, at lower reducing agent concentrations, the mechanism shifted to a Tafel-like mechanism [35,36]. The latter conclusion is analogous to that observed for the mechanism of the M^0-NPs catalyzed H_2 formation from BH_4- in aqueous solutions [38].

Acknowledgement

We are indebted to the PAZY Foundation for the grant that enabled this study. V. M. would like to offer her special thanks to the Ministry of Aliyah and Integration for its generous sponsorship.

Appendix A. Supplementary data

Supplementary material related to this article can be found, in the online version, at doi:https://doi.org/10.1016/j.apcatb.2018.08.040.

References

[1] M.B. Smith, J. March, March's Advanced Organic Chemistry: Reactions, Mechanisms, and Structure, 5th ed., Wiley-Interscience, New York, 2001.
[2] A.A. Meharg, J. Wright, D. Osborn, Sci. Total Environ. 251/252 (2000) 243–253.
[3] W.W. Mohn, Biodegradation and bioremediation of halogenated organic compounds, in: A. Singh, O.P. Ward (Eds.), Biodegrad. Bioremediation, Springer Berlin Heidelberg, Berlin, Heidelberg, 2004, pp. 125–148.
[4] C. Ding, J. He, Microb. Biotechnol. 5 (2012) 347–367.
[5] M. Salkinoja-Salonen, J. Uotila, J. Jokela, M. Laine, E. Sask, Environ. Health Perspect. 103 (1995) 63–69.
[6] (a) R.P. Schwarzenbach, T. Egli, T.B. Hofstetter, U. von Gunten, B. Wehrli, Annu. Rev. Environ. Resour. 35 (2010) 109–136;
(b) D.L. Sedlak, U. von Gunten, Science 331 (2011) 42–43.
[7] W.J. Chen, C.P. Weisel, J. Am. Water Works Assoc. 90 (1998) 151–163.
[8] J. Dojlido, E. Zbiec, R. Swietlik, Water Res. 33 (1999) 3111–3118.
[9] F.W. Pontius, J. Am. Water Works Assoc. 91 (1999) 46–58.
[10] S.D. Richardson, M.J. Plewa, E.D. Wagner, R. Schoeny, D.M. DeMarini, Mutat. Res. Rev. Mut. Res. 636 (2007) 178–242.
[11] (a) X. Zha, L. Ma, Y. Liu, RSC Adv. 6 (2016) 16323–16330;
(b) Z. He, Q. Wang, J. Sun, J. Chen, S. Song, Int. J. Electrochem. Sci. 6 (2011) 2932–2942;
(c) L.L. Lifongo, D.J. Bowden, P. Brimblecombe, Chemosphere 55 (2004) 467–476;
(d) X. Li, J. Ma, S. Yue, Adv. Mater. Res. 518–523 (2012) 2939–2943;
(e) L. Altamar, L. Fernández, C. Borras, J. Mostany, H. Carrero, B. Scharifker, Sens. Actuators B 146 (2010) 103–110;
(f) R. Mao, N. Li, H. Lan, X. Zhao, H. Liu, J. Qu, M. Sun, Environ. Sci. Technol. 50 (2016) 3829–3837;
(g) X. Li, J. Ma, G. Liu, J. Fang, S. Yue, Y. Guan, L. Chen, X. Liu, Environ. Sci. Technol. 46 (2012) 7342–7349;
(h) O. Scialdone, A. Galia, S. Sabatino, D. Mira, C. Amatore, ChemElectroChem. 2 (2015) 684–690;
(i) Y.H. Xu, H. Zhang, C.P. Chu, C.A. Ma, J. Electroanal. Chem. 664 (2012) 39–45;
(j) Q. Zhu, Y. Wang, H. Zhang, R. Duan, C. Chen, W. Song, J. Zhao, Appl. Catal. B 219 (2017) 322–328;
(k) A. Li, X. Zhao, Y. Hou, H. Liu, L. Wu, J. Qu, Appl. Catal. B 111-112 (2012) 628–635;
(l) Y. Albo, E. Shandalov, L. Hayoun, I. Zilbermann, E. Maimon, D. Meyerstein, Inorganica Chim. Acta 466 (2017) 502–509.
[12] (a) J. Adhikary, M. Meistelman, A. Burg, D. Shamir, D. Meyerstein, Y. Albo, Eur. J. Inorg. Chem. (2017) 1510–1515;
(b) M. Meistelman, J. Adhikary, A. Burg, D. Shamir, G. Gershinsky, D. Meyerstein, Y. Albo, Chim. Oggi Chem. Today 35 (2017) 23–26.
[13] (a) B. Hu, C. Wu, Z. Zhang, L. Wang, Ceram. Int. 40 (2014) 7015–7021;
(b) G. Moussavi, M. Rezaei, Chem. Eng. J. 328 (2017) 331–342;
(c) B. Liu, C. Ding, B. Xiao, L. Cui, M. Wang, Mater. Sci. Eng. C 37 (2014) 108–112;
(d) S. Tang, X. Wang, Y. Mao, Y. Zhao, H. Yang, Y.F. Xie, Water Res. 73 (2015) 342–352;
(e) R.M. Hozalski, L. Zhang, W. Arnold, Environ. Sci. Technol. 35 (2001) 2258–2263.
[14] (a) L.J. Matheson, P.G. Tratnyek, Environ. Sci. Technol. 28 (1994) 2045–2053; H. Li, Y. Q. Chen, S. Chen, X. L. Wang, S. Guo, Y. F. Qiu, Y. D. Liu, X. L. Duan, Y. J. Yu, DOI:10.1371/journal.pone.0172337.
(b) T. Li, J. Farrel, Environ. Sci. Technol. 34 (2000) 173–179;
(c) L. Zhang, W.A. Arnold, R.M. Hozalski, Environ. Sci. Technol. 38 (2004) 6881–6889;
(d) C. Scheutz, K. Winther, P. Kjeldsen, Environ. Sci. Technol. 34 (2000) 2557–2563;
(e) G.E. Hoag, J.B. Collins, J.L. Holcomb, J.R. Hoag, M.N. Nadagouda, R.S. Varma, J. Mater. Chem. 19 (2009) 8671–8677;
(f) L. Xu, J. Wang, J. Hazard. Mater. 186 (2011) 256–264;
(g) F. Fu, D.D. Dionysiou, H. Liu, J. Hazard. Mater. 267 (2014) 194–205;
(i) E.J.C. Borojovich, R. Bar-Ziv, O. Oster-Golberg, H. Sebbag, M. Zinigrad, D. Meyerstein, T. Zidki, Appl. Catal. B 210 (2017) 255–262;
(j) I. Rusonik, H. Cohen, D. Meyerstein, Inorg. Chem. 45 (2006) 7389–7396;
(k) S. Giri, M. Bhaumik, R. Das, V.K. Gupta, A. Maity, Appl. Catal. B 202 (2017) 207–216
[15] (a) D. Astruc, F. Lu, J.R. Aranzaes, Angew. Chem., Int. Ed. 44 (2005) 7852–7872;
(b) M. Stratakis, H. Garcia, Chem. Rev. 112 (2012) 4469–4506;
(c) B.K. Min, C.M. Friend, Chem. Rev. 107 (2007) 2709–2724;
(d) H. Cong, C.F. Becker, S.J. Elliott, M.W. Grinstaff, J.A. Porco Jr, J. Am. Chem. Soc. 132 (2010) 7514–7518;
(e) X.Y. Dong, Z.W. Gao, K.F. Yang, W.Q. Zhang, L.W. Xu, Catal. Sci. Technol. 5 (2015) 2554–2574;
(f) T. Mitsudome, S. Arita, H. Mori, T. Mizugaki, K. Jitsukawa, K. Kaneda, Angew. Chem. 120 (2008) 8056–8058;
(g) T.L. Tan, L.L. Wang, J. Zhang, D.D. Johnson, K. Bai, ACS Catal. 5 (2015) 2376–2383;
(h) L. Bai, X. Wang, Q. Chen, Y. Ye, H. Zheng, J. Guo, Y. Yin, C. Gao, Angew. Chem. Int. Ed. 55 (2016) 1–7;
(i) M. Conte, H. Miyamura, S. Kobayashi, V. Chechik, J. Am. Chem. Soc. 131 (2009) 7189–7196;
(j) S. Guo, X. Zhang, W. Zhu, K. He, D. Su, A. Mendoza-Garcia, S.F. Ho, G. Lu, S. Sun, J. Am. Chem. Soc. 136 (2014) 15026–15033.
[16] (a) M.K. Kundu, M. Sadhukhan, S. Barman, J. Mater. Chem. B 3 (2015) 1289–1300;
(b) J. Tian, Q. Liu, A.M. Asiri, A.H. Qusti, A.O. Al-Youbi, X. Sun, Nanoscale 5 (2013) 11604–11609;
(c) J. Tian, Q. Liu, C. Ge, Z. Xing, A.M. Asiri, A.O. Al-Youbi, X. Sun, Nanoscale 5 (2013) 8921–8924;

(d) L. Guo, Y. Xu, A.R. Ferhan, G. Chen, D.H. Kim, J. Am. Chem. Soc. 135 (2013) 12338–12345;
(e) S.S.R. Dasary, A.K. Singh, D. Senapati, H. Yu, P.C. Ray, J. Am. Chem. Soc. 131 (2009) 13806–13812.
[17] A.D. McFarland, R.P. Van Duyne, Nano Lett. 3 (2003) 1057–1062.
[18] Y. Zhang, G. Chang, S. Liu, J. Tian, L. Wang, W. Lu, X. Qin, X. Sun, Catal. Sci. Technol. 1 (2011) 1636–1640.
[19] (a) O. Lugaresia, J.V. Perales-Rondón, A. Minguzzi, J. Solla-Gullón, S. Rondinini, J.M. Feliu, C.M. Sánchez-Sánchez, Appl. Catal. B 163 (2015) 554–563;
(b) Y. Wang, Q. Zhu, Y. Wei, Y. Gong, C. Chen, W. Song, J. Zhao, Appl. Catal. B231 (2018) 262–268;
(c) A. Minguzzi, O. Lugaresi, G. Aricci, S. Rondinini, A. Vertova, Electrochem. Commun. 22 (2012) 25–28.
[20] (a) R. Ciriminna, G. Scandura, V. Pandarus, R. Delisi, A. Scurria, F. Beland, G. Palmisano, M. Pagliaro, ChemCatChem 9 (2017) 1322–1328;
(b) P.C. Marr, A.C. Marr, GreenChem. 18 (2016) 105–128;
(c) R. Ciriminna, A. Fidalgo, V. Pandarus, F. Béland, L.M. Ilharco, M. Pagliaro, ChemCatChem 7 (2015) 254–260;
(d) A.E. Danks, S.R. Hall, Z. Schnepp, Mater. Horiz. 3 (2016) 91–112.
[21] M.J. Frisch, G.W. Trucks, H.B. Schlegel, G.E. Scuseria, M.A. Robb, J.R. Cheeseman, G. Scalmani, V. Barone, B. Mennucci, G.A. Petersson, H. Nakatsuji, M. Caricato, X. Li, H.P. Hratchian, A.F. Izmaylov, J. Bloino, G. Zheng, J.L. Sonnenberg, M. Hada, M. Ehara, K. Toyota, R. Fukuda, J. Hasegawa, M. Ishida, T. Nakajima, Y. Honda, O. Kitao, H. Nakai, T. Vreven, J.A. Montgomery Jr, J.E. Peralta, F. Ogliaro, M. Bearpark, J.J. Heyd, E. Brothers, K.N. Kudin, V.N. Staroverov, R. Kobayashi, J. Normand, K. Raghavachari, A. Rendell, J.C. Burant, S.S. Iyengar, J. Tomasi, M. Cossi, N. Rega, J.M. Millam, M. Klene, J.E. Knox, J.B. Cross, V. Bakken, C. Adamo, J. Jaramillo, R. Gomperts, R.E. Stratmann, O. Yazyev, A.J. Austin, R. Cammi, C. Pomelli, J.W. Ochterski, R.L. Martin, K. Morokuma, V.G. Zakrzewski, G.A. Voth, P. Salvador, J.J. Dannenberg, S. Dapprich, A.D. Daniels, Ö. Farkas, J.B. Foresman, J.V. Ortiz, J. Cioslowski, D.J. Fox, Gaussian 09, Revision D.01, Gaussian, Inc., Wallingford, CT, 2013.
[22] M. Mantina, R. Valero, D.G. Truhlar, J. Chem. Phys. 131 (2009) 1–5.
[23] S. Brunauer, L.S. Deming, W.E. Deming, E. Teller, J. Am. Chem. Soc. 62 (1940) 1723–1732.
[24] (a) J. Adhikary, B. Das, S. Chatterjee, S.K. Dash, S. Chattopadhyay, S. Roy, J.W. Chen, T. Chattopadhyay, J. Mol. Struct. 1113 (2016) 9–17;
(b) R. Gupta, P.K. Rastogi, V. Ganesan, D.K. Yadav, P.K. Sonkar, Sens. Actuators B 239 (2017) 970–978.
[25] J.F. Moulder, W.F. Stickle, P.E. Sobol, K.D. Bomben, Handbook of X-ray Photoelectron Spectroscopy, Perkin-Elmer Corp., Eden Prairie, MN, USA, 1992.
[26] (a) S. Park, J.M. Lee, Y.K. Jo, I.Y. Kim, S.J. Hwang, Dalton Trans. 43 (2014) 10566–10573;
(b) S. Arii, F. Mortin, A.J. Renouprez, J.L. Rousset, J. Am. Chem. Soc. 126 (2004) 1199–1205.
[27] (a) S. Giri, R. Das, C. van der Westhuyzen, A. Maity, Appl. Catal. B 209 (2017) 669–678;
(b) S. Choi, Y. Jeong, J. Yu, RSC Adv. 6 (2016) 73805–73809;
(c) S. Fountoulaki, V. Daikopoulou, P.L. Gkizis, I. Tamiolakis, G.S. Armatas, I.N. Lykakis, ACS Catal. 4 (2014) 3504–3511.
[28] (a) R. Bar-Ziv, I. Zilbermann, T. Zidki, H. Cohen, D. Meyerstein, J. Phys. Chem. C 113 (2009) 3281–3286;
(b) I. Rusonik, T. Zidki, H. Cohen, D. Meyerstein, Glass Phys. Chem. 31 (2005) 115–118;
(c) O. Golberg-Oster, R. Bar-Ziv, G. Yardeni, I. Zilbermann, D. Meyerstein, Chem. Eur. J. 17 (2011) 9226–9231;
(d) R. Bar-Ziv, I. Zilbermann, T. Zidki, G. Yardeni, V. Shevchenko, D. Meyerstein, Chem. Eur. J. 18 (2012) 6733–6736.
[29] (a) T. Zidki, A. Hänel, R. Bar-Ziv, Radiat. Phys. Chem. 124 (2016) 41–45;
(b) R. Bar-Ziv, T. Zidki, I. Zilbermann, G. Yardeni, D. Meyerstein, ChemCatChem 8 (2016) 2761–2764;
(c) R. Bar-Ziv, I. Zilbermann, O. Oster-Golberg, T. Zidki, G. Yardeni, H. Cohen, D. Meyerstein, Chem. Eur. J. 18 (2012) 4699–4705.
[30] (a) R. van Eldik, D. Meyerstein, Acc. Chem. Res. 33 (2000) 207–214;
(b) S. Goldstein, G. Czapski, H. Cohen, D. Meyerstein, J.K. Cho, S.S. Shaik, Inorg. Chem. 31 (1992) 798–803;
(c) H. Cohen, D. Meyerstein, J. Chem. Soc. Faraday Trans. 1 (84) (1988) 4157–4160;
(d) H. Cohen, D. Meyerstein, Angew. Chem. Int. Ed. Engl. 97 (1985) 785–787.
[31] R. Levy-Yanus, G. Yardeni, E. Maimon, M. Saphier, I. Zilbermann, D. Meyerstein, Eur. J. Inorg. Chem. (2016) 1161–1164.
[32] K. Bobuatong, S. Karanjit, R. Fukuda, M. Ehara, H. Sakurai, Phys. Chem. Chem. Phys. 14 (2012) 3103–3111.
[33] S. Karanjit, M. Ehara, H. Sakurai, Chem. Asian J. 10 (2015) 2397–2403.
[34] K. Wiberg, Tetrahedron 24 (1968) 1083–1096.
[35] R. Jana, A. Bhim, P. Bothra, S.K. Pati, S.C. Peter, ChemSusChem 9 (2016) 2922–2927.
[36] Q. Tang, D. Jiang, ACS Catal. 6 (2016) 4953–4961.
[37] (a) N. Shaham, A. Masarwa, Y. Matana, H. Cohen, D. Meyerstein, Eur. J. Inorg. Chem. (2002) 87–92;
(b) S. Goldstein, G. Czapski, R. van Eldik, N. Shaham, H. Cohen, D. Meyerstein, Inorg. Chem. 40 (2001) 4966–4970.
[38] A. Sermiagin, R. Bar-Ziv, H. Cohen, D. Meyerstein, T. Zidki, unpublished results.
[39] R. Bar-Ziv, I. Zilbermann, M. Shandalov, V. Shevchenko, D. Meyerstein, Chem. Eur. J. 21 (2015) 19000–19009.
[40] (a) X. Liu, J. Zhong, L. Fang, L. Wang, M. Ye, Y. Shao, J. Li, T. Zhang, Chem. Eng. J. 303 (2016) 56–63;
(b) M.D. Esclapez, I. Tudela, M.I. Díez-García, V. Sáez, P. Bonete, Appl. Catal. B 166–167 (2015) 66–74;
(c) Y. Liu, R. Mao, Y. Tong, H. Lan, G. Zhang, H. Liu, J. Qu, Electrochim. Acta 232 (2017) 13–21.